ARTICLE   OPEN

Check for updates

Increasing atmospheric dust transport towards the western Mediterranean over 1948–2020

Pedro Salvador [1,✉], Jorge Pey [2,3], Noemí Pérez [4], Xavier Querol [4] and Begoña Artíñano [1]

In this study, global reanalysis dataset fields of meteorological parameters (temperature and geopotential height at different atmospheric levels) in the period 1948–2020, were used to characterize the main dynamic and thermodynamic features of African dust outbreaks (ADO) produced over regions of the Iberian Peninsula and the Balearic Islands. The record of ADO previously identified with a tried-and-true procedure in 8 different areas of this domain in the period 2001–2020 and the data sets of dust load contributions estimated for all ADO days in each region, were used to check our results. Thus, we demonstrated that air masses of African origin produced a significant increase in the levels of certain thermodynamic variables (geopotential thickness in the 1000–500 hPa layer (GT), mean potential temperature between 925 and 700 hPa (TPOT), and temperature anomalies at 850 hPa (TANOM)) over the regions of study, especially when particular synoptic-scale atmospheric circulation types (CT) occurred. Moreover, higher levels of the three thermodynamic parameters resulted in events with higher contributions of dust load to the regional background levels of PM_{10} in all regions. Finally, we obtained a statistically significant upward trend for days under ADO CT and their associated daily mean values of GT, TPOT and TANOM from 1948 to 2020. These results point to an increase in the frequency of air mass transport from North Africa to the western Mediterranean basin and on the intensity of the ADO produced as a consequence of this transport, over 1948–2020.

INTRODUCTION

The extension of desert areas in subtropical latitudes of both hemispheres is increasing[1]. It has been estimated that the Sahara desert has expanded 10% on average in the period 1920–2013[2]. Such expansion mainly reached the Sahel region in summer and the northern borderline of the African mainland in winter. In this sense, it is currently assumed that since 1950s different human activities including overgrazing and agriculture have exacerbated or provoked the desiccation of playas and ephemeral lakes located over the northern Sahara and the Sahel, overall reactivating eolian processes[3]. These potential source areas of dust were considered as anthropogenic sources, i.e. associated with some form of land use, as interpreted from satellite products[4]. Moreover, dust emissions from desert regions are very sensitive to weather and climate conditions in source areas[5]. Hence, the gradual increase in temperatures and periods of drought together with changes in land uses, probably made soil more sensitive to erosion that, in turn, is a cause of dust storms[3,6]. As a consequence, important year-to-year changes in the frequency of dust storms over Sahara and Sahel regions were detected during the second half of the 20th century[5–7]. Besides, the magnitude and poleward extension of advections of very warm Saharan air masses have also risen in the second half of the 20th century[8].

In relation to these findings, a long-term increase in Saharan dust flux was obtained over western Europe, by means of speleothem strontium isotope ratios and karst modelling[9]. Positive trends in African dust transport have also been detected after 1980 over the subtropical Eastern North Atlantic[10] and the Carpathian Basin (central Europe)[11]. Such increases were attributed to progressive north Africa aridification and/or to changes in the synoptic atmospheric circulation. Otherwise, a statistically significant downward trend for the dust optical depth over the tropical north Atlantic was determined from the mid-1980s[12]. A reduction for the dust optical depth in this region was also forecasted along the twenty-first century using a climate model[12]. It is thus clear that there are still discrepancies and uncertainties regarding the past and future evolution of long-range transport processes of African dust.

African dust has been intensely analysed from an air quality matter perspective. Since the 90 s vast numbers of studies have shown that African dust is the main input from a natural source contributing to increase regional background levels of PM_{10} in Southern Europe[13–15]. It has also been demonstrated that the occurrence of African dust outbreaks (ADO) trigger exceedances of the PM_{10} daily limit value for the protection of health (set at 50 μg/m³ in EU Directive 2008/50/EC on ambient air quality and a cleaner atmosphere in Europe) at rural, suburban and urban air quality monitoring stations[15–17] and increases mortality and morbidity[18–21] in Southern European countries. Otherwise, ADO can also trigger ecosystem imbalances in the western Mediterranean basin. Wet and dry Saharan dust deposition events induced contrasting responses of the phytoplanktonic community in the north-western Mediterranean Sea, due to differences in the atmospheric supply of bioavailable new nutrients[22]. There were also detected changes in diatom composition produced by an increased Saharan dust deposition in remote lakes in the Sierra Nevada Mountains of southern Spain[23]. Thus, increasing trends in the occurrence of ADO in this region could exacerbate the harmful effects on human health and ecosystems, which could even get worse in the next years. For this reason, the long-term evaluation

[1]CIEMAT, Department of Environment - Joint Research Unit Atmospheric Pollution CIEMAT-CSIC, Av. Complutense 40, 28040 Madrid, Spain. [2]Fundación Agencia Aragonesa para la Investigación y el Desarrollo – ARAID, Av. Ranillas 1-D, 50018 Zaragoza, Spain. [3]Instituto Pirenaico de Ecología (IPE), CSIC, Av. Montañana 1005, 50059 Zaragoza, Spain. [4]Institute of Environmental Assessment and Water Research (IDAEA), CSIC, Jordi Girona 18, 08034 Barcelona, Spain. ✉email: pedro.salvador@ciemat.es

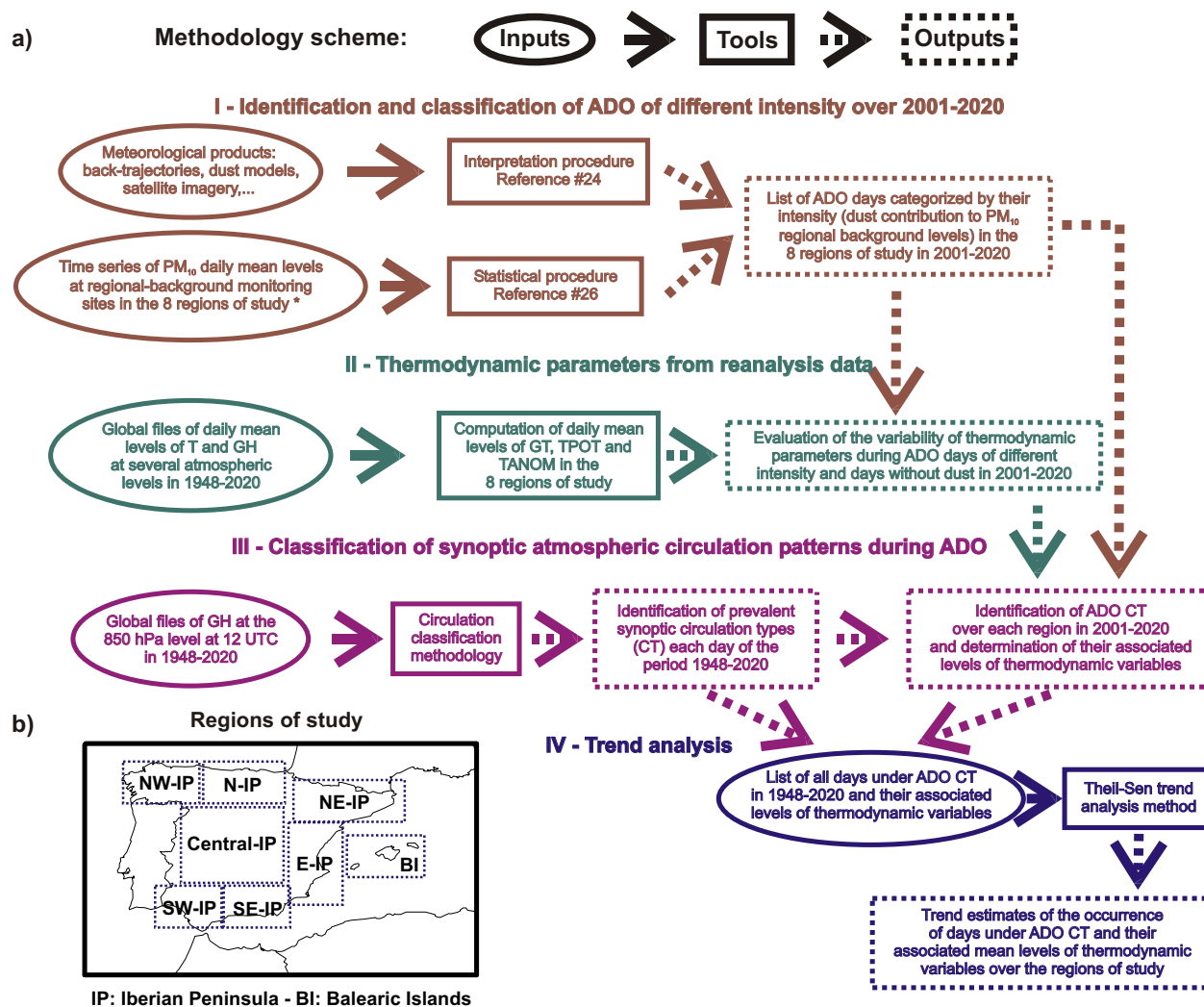**a)** Methodology scheme: Inputs ➤ Tools ➤ Outputs

I - Identification and classification of ADO of different intensity over 2001-2020

Meteorological products: back-trajectories, dust models, satellite imagery,... ➤ Interpretation procedure Reference #24

Time series of PM_{10} daily mean levels at regional-background monitoring sites in the 8 regions of study * ➤ Statistical procedure Reference #26

List of ADO days categorized by their intensity (dust contribution to PM_{10} regional background levels) in the 8 regions of study in 2001-2020

II - Thermodynamic parameters from reanalysis data

Global files of daily mean levels of T and GH at several atmospheric levels in 1948-2020 ➤ Computation of daily mean levels of GT, TPOT and TANOM in the 8 regions of study ➤ Evaluation of the variability of thermodynamic parameters during ADO days of different intensity and days without dust in 2001-2020

III - Classification of synoptic atmospheric circulation patterns during ADO

Global files of GH at the 850 hPa level at 12 UTC in 1948-2020 ➤ Circulation classification methodology ➤ Identification of prevalent synoptic circulation types (CT) each day of the period 1948-2020 ➤ Identification of ADO CT over each region in 2001-2020 and determination of their associated levels of thermodynamic variables

IV - Trend analysis

List of all days under ADO CT in 1948-2020 and their associated levels of thermodynamic variables ➤ Theil-Sen trend analysis method

Trend estimates of the occurrence of days under ADO CT and their associated mean levels of thermodynamic variables over the regions of study

b) Regions of study

NW-IP N-IP NE-IP
Central-IP E-IP BI
SW-IP SE-IP

IP: Iberian Peninsula - BI: Balearic Islands

Fig. 1 Methodological scheme. Flow chart showing the stages of the methodology used in this study (**a**) and regions of study (**b**). ADO African dust outbreaks, BI Balearic Islands, IP Iberian Peninsula.

of African dust transport towards southern European regions is a demand necessary to prevent future impacts.

In Spain, all ADO contributing to increase the regional-background levels of PM_{10} at regions of the Iberian Peninsula (IP), the Balearic Islands (BI) and the Canary Islands have been identified from 2001 to 2020 using a well-known procedure[24,25]. However, the meteorological tools (air mass back-trajectories, satellite imagery and numerical models for prediction of dust levels) and databases (time series of PM levels registered at regional background air quality monitoring stations) needed to perform the identification procedure are scarce before the year 2000. This is the reason why the occurrence of ADO in these regions during the former decades has not been well addressed so far.

To overcome such important lack of information, in this study we discern the main distinctive synoptic dynamic and thermodynamic features associated to African dust export towards regions of the western Mediterranean basin, the IP and the BI, with the objective of detecting temporal trends over 1948–2020. This trend analysis would help elucidating whether ADO have been aggravating over the years (in frequency and/or intensity) or not. In addition, such synoptic characterization based on meteorological parameters could be used for evaluating the future evolution of this extreme meteorological event by means of weather and/or climate models.

This work is organized as follows (Fig. 1):

First, we identified all the dates when ADO happened on each of the 8 study areas (the BI and the southeastern (SE), southwestern (SW), eastern (E), Central, northwestern (NW), northern (N) and northeastern (NE) regions of the IP, Fig. 1) in the period 2001–2020. The data sets of daily net dust load contributions to the regional background levels of PM_{10} were also obtained for each ADO day. Then, we calculated the daily mean values of a number of specific thermodynamic parameters, which could be used to detect the presence of African air masses in this period. The objective was to test the relationship between the occurrence and intensity of ADO and the deviation of these thermodynamic parameters above their normal values. Next, the main synoptic circulation patterns that drove the occurrence of ADOs in 2001–2020 over each study region were identified and the associated mean values of thermodynamic parameters were also evaluated. The objective of this task was to inspect the existence of interconnections between the main synoptic dynamic and thermodynamic features of the ADO developed over the IP-BI domain. It would demonstrate that atmospheric circulation patterns and thermodynamic variables could be used to characterise the occurrence of ADO in this region of the Mediterranean basin. Finally, the information obtained in the previous tasks was used to investigate the evolution over time of the main synoptic meteorological conditions that favour ADO, in

order to detect upward or downward trends that could have happened in the period 1948–2020.

RESULTS AND DISCUSSION

Values adopted by thermodynamic parameters during ADO

Median values of mean potential temperature between 925 and 700 hPa (TPOT), temperature anomalies at 850 hPa (TANOM) and geopotential thickness in the 1000–500 hPa layer (GT) over each of the 8 sub-domains during ADO days and days without dust contribution (non-ADO) for the period 2001–2020 are shown in Fig. 2. Mean and median values of these variables in this period, studying separately winter (Dec-Jan-Feb), spring (Mar-Apr-May), summer (Jun-Jul-Aug) and autumn (Sep-Oct-Nov) seasons can be found in Supplementary Tables 1, 2.

Statistically significant differences between the medians and the shape of the distributions corresponding to ADO and non-ADO days were obtained over all regions and seasons at the 95% confidence level. It has been demonstrated that intrusions of Saharan air masses are key drivers of summer heatwaves affecting the IP, particularly those affecting the southernmost sectors[8]. Our results bring out that the occurrence of ADO is accompanied by a significant increase in levels of TPOT, TANOM and GT throughout all the year and in all regions, and not exclusively in summer during the development of heat waves, when they reach very extreme values.

A detailed analysis of 4 ADO affecting the western Mediterranean during different seasons of the year and under different atmospheric circulation patterns has been included as Supplementary Note 1. They were considered intense events because the daily dust contribution to the PM_{10} regional background levels exceeded the average dust value obtained for all ADO during 2001–2020 by at least 25% in at least 4 out of the 8 study regions. It is based on synoptic maps of levels of the three thermodynamic parameters, 850 hPa geopotential height, optical depth and dust concentration (Supplementary Figs 1, 2 and 3, respectively). This analysis suggests that the presence of African air masses over regions of the IP-BI domain can be retrieved when high values of TPOT, TANOM and GT in the corresponding maps are encountered. These maps also represented the main synoptic features (high-pressure systems, cyclonic areas, troughs,…) that characterized the meteorological situation that generated the dust transport.

Connection between intensity of ADO and thermodynamic variables

The relationship between the values adopted by TPOT, TANOM and GT and the intensity of the ADO identified over the period 2001–2020, considering as such the load of dust in PM_{10} concentrations, was investigated. The mean and median values of TPOT, TANOM and GT for ADO days of increasing intensity in all study areas are provided as supplementary information (Supplementary Table 3). In general, higher mean levels of the 3 variables were obtained in all areas at higher event intensities. That is, higher values of TPOT, TANOM and GT resulted in events with higher contributions of dust load to the regional background levels of PM_{10}. The Kruskal-Wallis test determined that in all cases there were statistically significant differences in TPOT, TANOM and GT medians as a function of event intensity at a 95% confidence level. Only in 2 areas (SE-IP and NW-IP) the differences between the medians for the variable GT were statistically significant at a lower confidence level of 90%. It must be taken into account that African dust may contribute to increase surface PM_{10} levels in regions of the IP-BI domain some days after the African air masses have left this region. The reason for this is the fact that the complete removal of African dust in the atmosphere can last 2–3 days, especially when African air masses travel at high altitudes[26,27]. The procedure used to identify ADO days[24] takes into account such persistence effect and therefore they are considered as ADO days. Bearing this in mind, a perfect linear regression between the daily levels of dust contribution and those of TPOT, TANOM and GT could not occur. Figure 3 shows the daily mean values of TANOM in all areas during ADO of increasing intensity. A gradual rise in TANOM levels was evident as the atmospheric dust load during the African episodes increased.

In addition, it has been ascertained a clear negative latitudinal gradient for the mean values of TPOT and GT, which contrast to a positive latitudinal gradient for TANOM values during ADO of increasing intensity (Fig. 4). The R^2 of the linear regressions ranged from 0.72 to 0.97 in all the cases. All ADO, regardless of their intensity, have been associated with higher values of TPOT and GT and lower values of TANOM in southern regions of the IP, than in the central area of the IP and the BI and in areas of the northern sectors of the IP. Such inverse behavior of TANOM with respect to TPOT and GT could be explained by the fact that the proximity of southern IP regions to North African deserts make these areas more liable to the advent of warm and dusty air masses[15], overall explaining the lower TANOM values observed here when compared with areas more rarely affected by such warm air masses. These results show a clear relationship between the amplitude of the considered meteorological thermodynamic parameters and the intensity of the events.
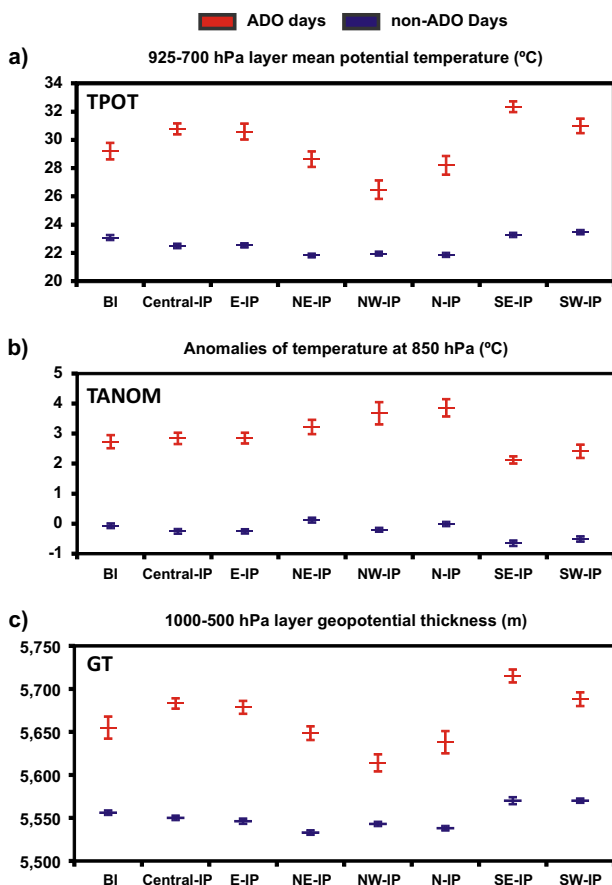

Fig. 2 Impact of ADO on thermodynamic parameters. Median values (and 95% confidence intervals) of TPOT (**a**), TANOM (**b**), and GT (**c**) over each of the 8 regions of study during ADO days and days without dust contribution (non-ADO) in the period 2001–2020. BI Balearic Islands, IP Iberian Peninsula.
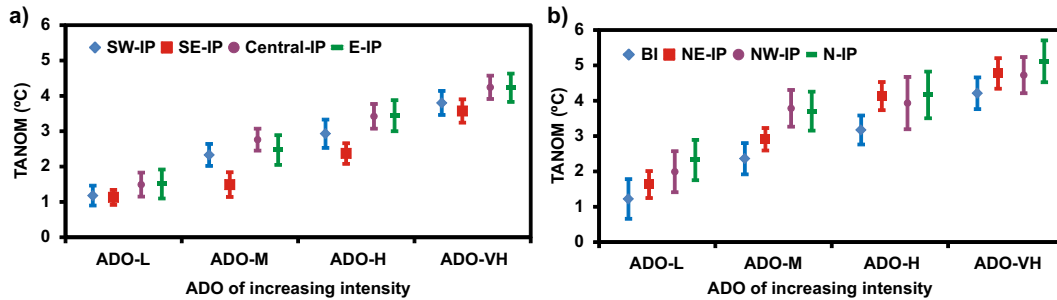
Fig. 3 Impact of ADO of increasing intensity on thermodynamic parameters. Median values (and 95% confidence intervals) of anomalies of temperature at 850 hPa (TANOM in °C), in the SW, SE, Central and E regions of the IP (**a**) and in the BI and the NE, NW and N regions of the IP (**b**) during ADO of increasing intensity in the period 2001–2020. ADO-L low event, ADO-M moderate event, ADO-H high event, ADO-VH very high event, IP Iberian Peninsula, BI Balearic Islands.
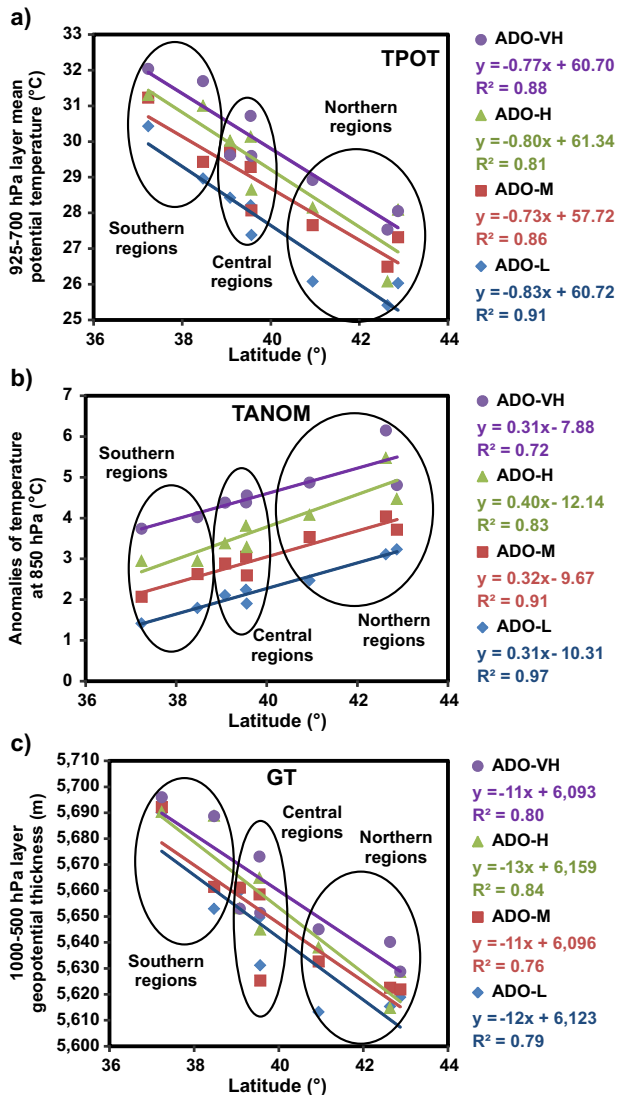

Fig. 4 Variation of the thermodynamic parameters with the latitude during ADO. Linear regressions between the latitudes of the regional background air quality monitoring stations and the mean values of TPOT (**a**), TANOM (**b**) and GT (**c**) registered over each region of study during ADO of different intensity in the period 2001–2020. ADO-L low event, ADO-M moderate event, ADO-H high event, ADO-VH very high event.

Atmospheric circulation patterns and thermodynamic parameters during ADO

The classification of the atmospheric circulation scenarios using clustering techniques unveiled 11 different circulation-types (CT). A full description of their main characteristics and their relationship with ADO has been included as supplementary material (Supplementary Table 4 and Supplementary Figs 4–6). Development of ADO over the period 2001–2020 was mostly produced under 6 specific CT (> 90% of the ADO days in all regions during CT-I, CT-II, CT-IV, CT-VI, CT-VIII, and CT-X, Fig. 5). They are akin to those reported in previous studies as the main drivers of ADO over the western Mediterranean basin[14–16,28,29]. The 4 ADO described in Supplementary Figs 1–3 were produced under CT-I, CT-X, CT-II, and CT-IV, respectively. The other CTs identified have described advections of air masses from different sectors of the Atlantic Ocean (NW: CT-III and CT-XI, N-NW: CT-IX and W: CT-VII) or from the European continent (CT-V), and have therefore not been associated with the development of ADO over the western sector of the Mediterranean basin (Fig. 6 and Supplementary Table 4).

What is important to note is that the daily mean levels of TANOM, GT and TPOT recorded in all study areas during ADO CT were in general higher than those recorded when the other types of circulation patterns happened (Fig. 7 and Supplementary Table 5). The Kruskal-Wallis test determined that in all regions there were statistically significant differences in medians of daily levels of TPOT, TANOM and GT corresponding to days under each of the 11 CT at a 95% confidence level. The highest median values of the three thermodynamic parameters with statistical significance corresponded in all regions of study to ADO CT. In the case of GT and TPOT, the highest median values in the 8 areas corresponded to the most frequent patterns, CT-I and CT-X (Fig. 7a and b). The other ADO circulation patterns, CT-II, CT-IV, CT-VI and CT-VIII, have presented lower median values of GT and TPOT, but they have also been higher than those corresponding to the rest of the circulation patterns. For TANOM, the highest median values were obtained for CT-VI in most study areas, followed by those corresponding to the other ADO CT with small differences between them, depending on the region (Fig. 7c). On the other hand, the CT-V, CT-VII, CT-IX and CT-XI patterns, not associated with the development of ADO, showed much lower daily median values of TANOM, very close to 0 or even negative, in all the areas studied.

In short, it seems clear that the ADO CT are associated with above-average levels of the thermodynamic variables TPOT, TANOM and GT registered over different areas of the IP-BI region. Such increases varied depending on the thermodynamic variables, the geographical location and the ADO CT. Moreover, the prevailing ADO CT and their frequency of occurrence changed depending on the period of the year.
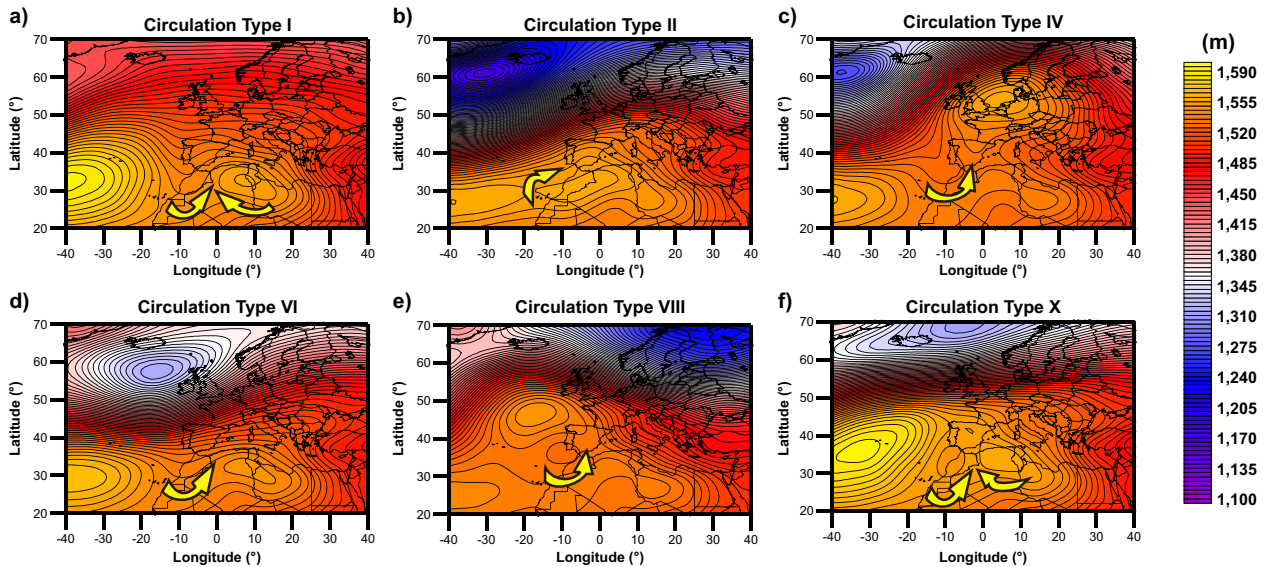
Fig. 5 Synoptic maps describing ADO circulation types. Composite synoptic maps of 850 hPa geopotential height at 12 UTC (m) for ADO circulation types (CT-I (**a**), CT-II (**b**), CT-IV (**c**), CT-VI (**d**), CT-VIII (**e**) and CT-X (**f**)) resulting from the circulation classification process, for the period 1948–2020. Arrows indicate the prevailing advection of the air masses towards the IP-BI domain.

Trends in circulation patterns and thermodynamic parameters during ADO

A statistically significant positive linear trend has been obtained for the number of days under ADO CT expressed as a slope of 0.77 days per year (Table 1). This result points to 55 ADO days more in 2020 with respect to 1948. The values of the thermodynamic parameters averaged over the IP-BI domain during days under any ADO circulation type also displayed statistically significant increasing trends (0.41 m year^{-1} for GT and 0.02 °C year^{-1} for TPOT and TANOM). In seasonal terms, the number of days under ADO CT and the mean levels of GT, TPOT and TANOM showed again statistically significant positive trends for summer, spring and winter periods (Table 1).

Thereafter, we evaluated the overall tendency and the seasonal trends for each specific CT giving rise to ADO (Table 2). The most frequent ADO circulation patterns, CT-I and CT-X, were the ones displaying the highest significant upward trends, 0.35 and 0.16 days year^{-1}, respectively. For the CT-II and CT-VI patterns, upward trends have also been obtained although with a smaller magnitude, 0.12 and 0.08 days year^{-1}, and lower confidence level. For CT-IV and CT-VIII the resulting trends were also positive (0.03 and 0.05, respectively) but not statistically significant. By season, statistically significant increasing trends were obtained for CT-I and CT-X in summer, and for CT-II in winter. As discussed above, summer concentrates most of CT-I and CT-X, and winter most of CT-II events. The rest of the patterns occurred more evenly throughout the year and probably for this reason the slight upward trends detected are seasonally smoothed.

Likewise, we have estimated the seasonal trends of the monthly mean levels of TPOT, TANOM and GH averaged over the IP-BI domain when ADO CT happened in the period 1948–2020 (Table 2). Positive trends of TPOT, TANOM and GH have been obtained in summer for CT-I, CT-IV, CT-VI and CT-X, in spring for CT-I and CT-IV and in winter for CT-II (Supplementary Figs 7, 8 and 9, respectively). Finally, no statistically significant trends were obtained for any seasonal period for CT-VIII.

Our findings unveil that values of thermodynamic parameters, which are directly associated with the intensity of ADO, have increased since 1948 onwards for most ADO CT occurring in summer, regardless of whether or not their frequency of occurrence has significantly risen over 1948–2020 (Table 2). The

same pattern occurred for specific CTs in spring (CT-IV) and winter (CT-II). These results would be in good agreement with the long-term increase in Saharan dust flux detected over Western Europe[9].

It should be taken into account that a statistically significant upward long-term trend in the air temperature at the 850 hPa level was detected over the IP-BI domain along the period 1948–2020 (0.02 K year^{-1}) which was more pronounced from the 1970s onwards (Fig. 8). The magnitude of the increasing trend was higher in summer (0.03 K year^{-1}) than in spring (0.02 K year^{-1}) and winter (0.02 K year^{-1}). Again, no statistically significant trend was detected in autumn for this meteorological variable. A surface temperature warming in the Northern Hemisphere has also been observed from the 1970s and some authors suggested that at least part of this trend may be the result of increasing greenhouse gas concentrations, i.e. the climate change[30,31]. Presently, it is unequivocally assumed that human influence has warmed the atmosphere, ocean and land over the 20th century and that most of the surface warming occurred during two periods, 1910 to 1945 and 1976 to 2000[32]. However, the smoothed trends obtained for all circulation types indicate that the increase of temperature at the 850 hPa level was mainly driven by the increasing frequency of ADO circulation types during spring, summer and winter. Unlike them, the other circulation types showed mostly stable or decreasing trends with lower values of temperature than the overall trend for 1948–2020 (Fig. 8). These results confirm the increase of ADO-related dynamic and thermodynamic influences over the IP-BI since 1948, which are closely connected with the observed increase in the air temperature at this atmospheric level. In fact, ADO circulation types showed trends with higher values of air temperature at the 850 hPa level in spring, summer and winter than the overall trend determined for 1948–2020 over the IP-BI domain. These findings show the link between the aggravation of warm conditions registered in southern Europe in the last decades and the increasing trend in frequency and intensity of ADO in this region, which could be an additional consequence of current human-derived climate change.

Climate change has been frequently associated with an exacerbation in the development of extreme weather events, such as droughts, floods or heat waves, in many regions of the earth. In this study, it has been directly related as well with an increase in the frequency and intensity of ADO over a given
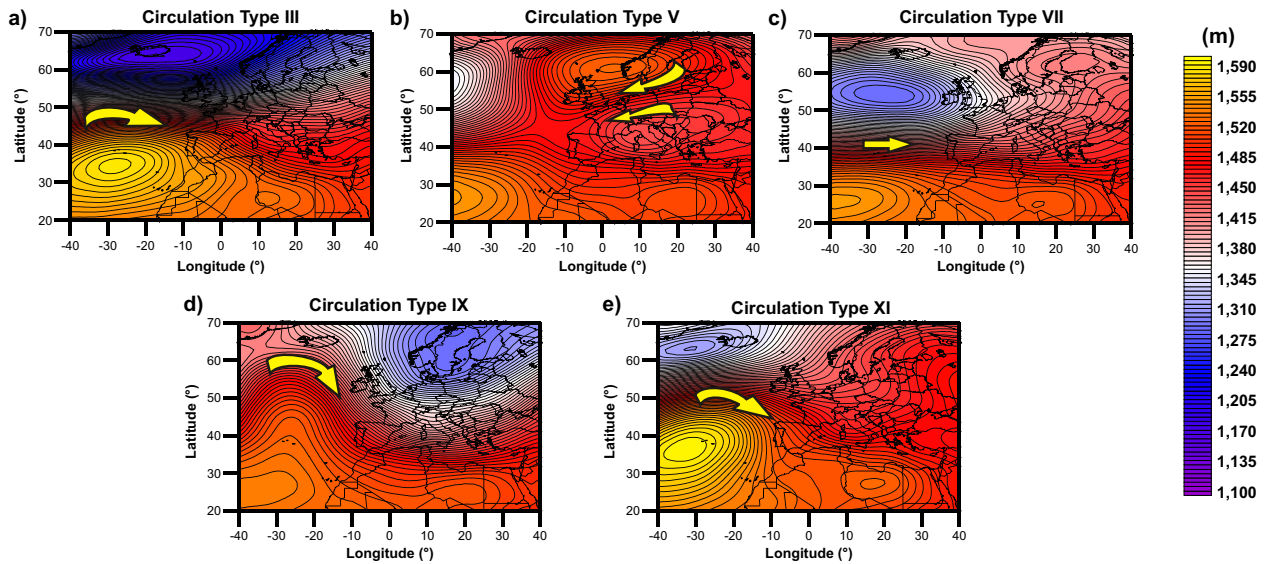
Fig. 6 Synoptic maps describing non-ADO circulation types. Composite synoptic maps of 850 hPa geopotential height at 12 UTC (m) for circulation types (CT-III (**a**), CT-V (**b**), CT-VII (**c**), CT-IX (**d**) and CT-XI (**e**)) resulting from the circulation classification process, which were not associated with the development of ADO, for the period 1948–2020. Arrows indicate the prevailing advection of the air masses towards the IP-BI domain.
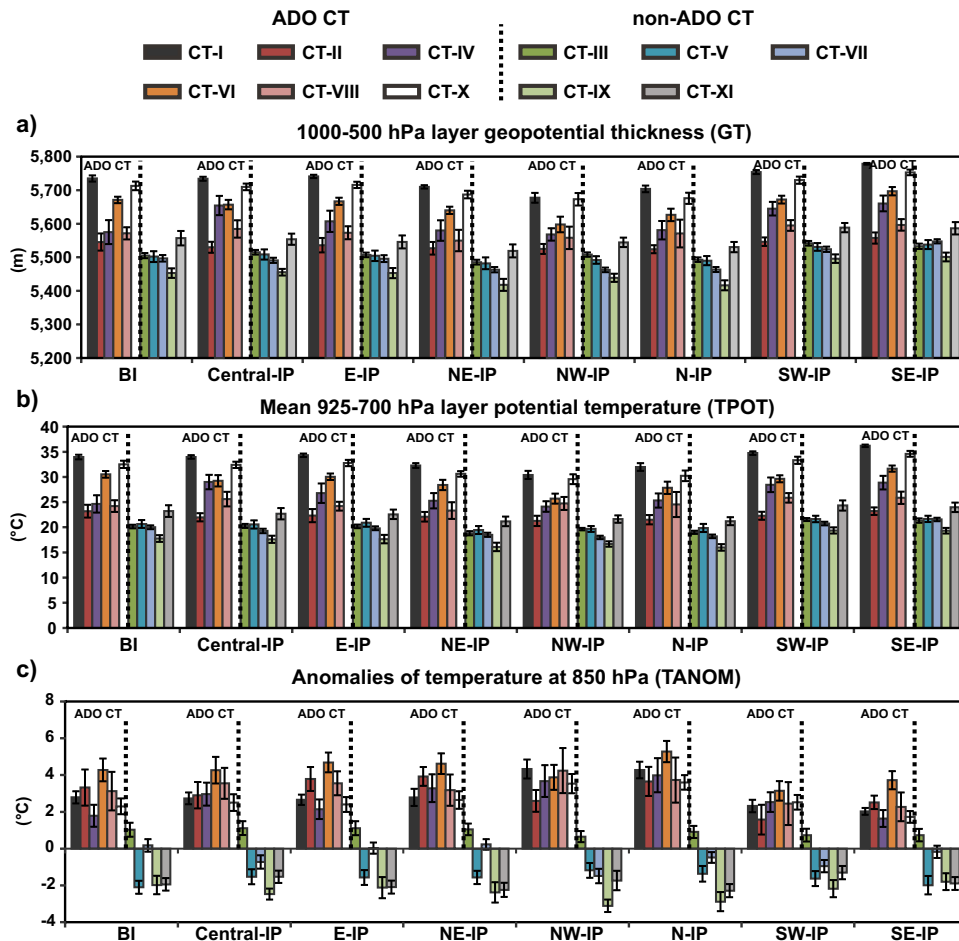

Fig. 7 Variation of the thermodynamic parameters with ADO and non-ADO circulation types. Median values (and 95% confidence intervals) of GT (**a**), TPOT (**b**) and TANOM (**c**) over each region of study under each atmospheric circulation type (CT) in the period 2001–2020.

Table 1. Trend analysis for days under any ADO CT for the 1948–2020 period.

Days under ADO CT	Number of days	GT	TPOT	TANOM
All days	0.77***	0.41**	0.02**	0.02**
Spring	0.98**	0.39*	0.02*	0.02***
Summer	0.78**	0.52***	0.04***	0.03***
Autumn	NT	NT	NT	0.02***
Winter	0.67*	0.38***	0.02***	0.02*

Results of the Theil-Sen trend analysis. Values of the Slope estimator in days year⁻¹, for the number of days under ADO atmospheric circulation types (ADO CT) and the mean levels of GT (m year⁻¹), TPOT (°C year⁻¹) and TANOM (°C year⁻¹) averaged over the Iberian Peninsula and the Balearic Islands during those days. ***, **, * and +: statistically significant value at the 99.9%, 99%, 95% and 90% confidence level, respectively, NT: no trend.

Table 2. Trend analysis for days under specific ADO CT for the 1948–2020 period.

ADO CT	All days	Spring	Summer	Autumn	Winter
Number of days under ADO CT					
CT-I	0.35***	NT	1.04***	NT	NT
CT-II	0.12+	NT	NT	NT	0.18+
CT-IV	NT	NT	NT	NT	NT
CT-VI	0.08+	NT	NT	NT	NT
CT-VIII	NT	NT	NT	NT	NT
CT-X	0.16*	NT	0.23+	NT	NT
GT: geopotential thickness in the 1000–500 hPa layer					
CT-I	0.38*	0.53+	0.59***	NT	NT
CT-II	NT	NT	NT	NT	0.29***
CT-IV	NT	0.55*	0.83***	NT	NT
CT-VI	NT	NT	0.39*	NT	NT
CT-VIII	NT	NT	NT	NT	NT
CT-X	0.22+	NT	0.52*	NT	NT
TPOT: mean potential temperature between 925 and 700 hPa					
CT-I	0.03**	0.03*	0.04***	NT	NT
CT-II	NT	NT	NT	NT	0.02+
CT-IV	NT	0.03*	0.05***	NT	NT
CT-VI	NT	NT	0.03*	NT	NT
CT-VIII	NT	NT	NT	NT	NT
CT-X	NT	NT	0.03***	NT	NT
TANOM: temperature anomalies at 850 hPa					
CT-I	0.03***	0.03***	0.04***	0.02+	NT
CT-II	0.02***	NT	NT	NT	0.02*
CT-IV	0.02***	0.03**	0.05***	NT	NT
CT-VI	0.02***	0.02*	0.02**	0.02*	NT
CT-VIII	0.02**	0.03*	NT	NT	NT
CT-X	0.02***	0.03*	0.03***	NT	NT

Results of the Theil-Sen trend analysis. Values of the Slope estimator in days year⁻¹, for the number of days under specific ADO atmospheric circulation types (ADO CT) and for the monthly mean levels of GT (m year⁻¹), TPOT (°C year⁻¹) and TANOM (°C year⁻¹) averaged over the Iberian Peninsula and the Balearic Islands during ADO CT. ***, * and +: statistically significant value at the 99.9%, 95% and 90% confidence level, respectively, NT: no trend.

region, such as the western Mediterranean basin. It is therefore clear that in order to reduce the adverse health effects produced during dust episodes in this region, reliable forecasting systems of the occurrence of ADO such as the Copernicus Atmospheric Monitoring Service or the World Meteorological Organisation Sand and Dust Storm Advisory and Assessment System will be instrumental to alert the authorities responsible for public health and air quality control. This way, protective and adaptive measures could be taken for the affected population. Otherwise, the synoptic characterization of ADO obtained as a result of this study is based on the identification of atmospheric circulation patterns and levels of thermodynamic parameters calculated from basic meteorological variables. Therefore, they could be implemented for forecasting in numerical weather prediction models as well as in climate models. In this way, the future evolution, in terms of intensity and frequency, of ADO in this region of study could be evaluated in the same way as is currently being done for other extreme weather events.

METHODS

Identification and classification of ADO of different intensity

A robust procedure based on the daily interpretation of several meteorological products, all them calculated or obtained from open access repositories, was used to identify all the ADO days with impact in the levels of PM_{10} registered in the 8 regions of study for the period 2001–2020[24]. Firstly, back-trajectories of air masses are interpreted to account for the transport of air masses from N Africa. Secondly, aerosol maps from numerical models and satellite images are evaluated, which usually result in the consideration of additional days impacted by dust. For specific cases in which some doubts arise, meteorological maps are calculated to verify the existence of favourable scenarios for the transport of dust. Finally, time series of PM_{10} levels registered at regional background monitoring sites from the EMEP (European Monitoring and Evaluation Programme) and other regional air quality networks in each area (Supplementary Fig 10a) were obtained and used to validate the real impact of dust on surface PM_{10} levels.

These time series were also used to quantify the net African dust contribution on the PM_{10} daily records following a statistical procedure[26,33] recommended by the European Commission as one of the official methods for evaluating the occurrence of ADO and quantifying the surface dust contributions[27]. This method is based on the application of 30 days moving 40th percentile to the regional background PM_{10} daily data series, after excluding those days impacted by African dust. This percentile is an indicator of the non-African regional background to be subtracted from the daily PM_{10} levels during ADO, and thus allows calculating the absolute African dust contribution to PM_{10}. Daily dust contributions were thus used to categorize the degree of intensity of ADO in four categories: low (ADO-L), if the daily dust load level was less than or equal to the 25th percentile of the data series for the whole period; moderate (ADO-M), if the value was between the 25th and 50th

percentile; high (ADO-H), if it was between the 50th and 75th percentile; and very high (ADO-VH), if it was greater than or equal to the 75th percentile. Finally, a list of ADO with impact in the PM_{10} regional background levels in the 8 regions of study in the period 2001–2020 was created for subsequent analysis.

Thermodynamic parameters obtained from reanalysis data

Annual global fields of daily mean temperature and geopotential height at 17 pressure levels were obtained for the period 1948–2020. These data fields were downloaded from the National Centers for Environmental Prediction/National Centre for Atmospheric Research (NCEP/NCAR) Reanalysis dataset[34] provided by NOAA/OAR/ESRL PSD, USA. Data were distributed in each field in a 2.5° latitude x 2.5° longitude global grid (90°N - 90°S, 0°E - 357.5°E).

Then, we calculated for each day in the 8 sub-domains (Supplementary Fig 10b) the daily mean values of:

- Geopotential thickness in the 1000–500 hPa layer (GT).
- Mean potential temperature between 925 and 700 hPa (TPOT).
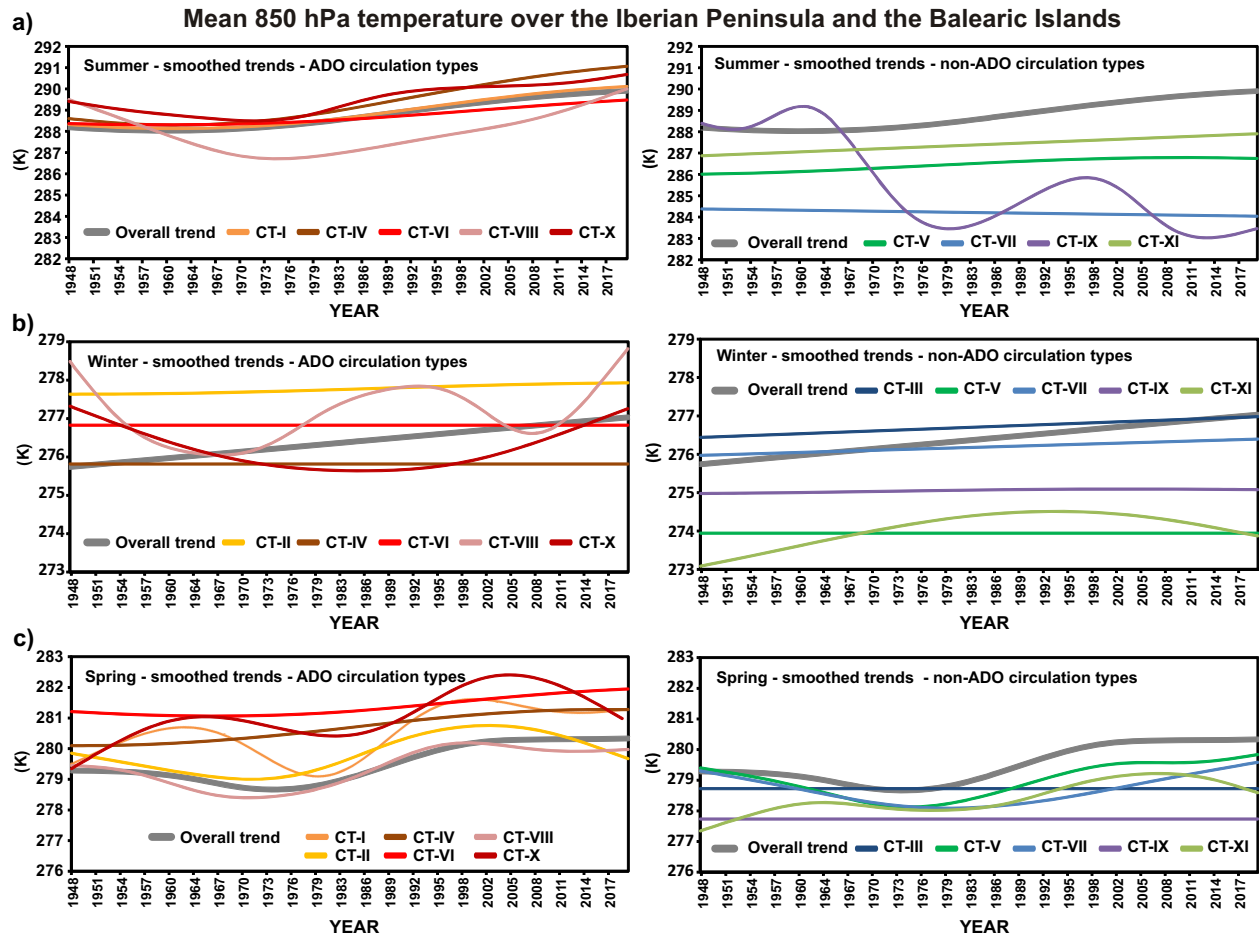- Temperature anomalies at 850 hPa relative to the climatological period 1981–2010 (TANOM).

Mean 850 hPa temperature over the Iberian Peninsula and the Balearic Islands

Fig. 8 Time evolution of temperature at 850 hPa over the IP and the BI domain over 1948–2020. Smoothed trend of the monthly mean levels of temperature at 850 hPa averaged over the Iberian Peninsula and the Balearic Islands in the period 1948–2020 (overall trend) and during the occurrence of the 8 circulation types (CT) obtained from the circulation classification process in summer (**a**), winter (**b**) and spring (**c**).

The selection of these parameters was not arbitrary, as high values of these indicators are usually related to warm, stable and dry air masses, i.e. with a probable origin in desert areas of N Africa[35,36]. Actually, different studies have identified incursions of warm and dry African air and, as a consequence, the development of summer heatwaves in areas of the IP, with high values of these parameters[8,37]. Then, the values of GT, TANOM and TPOT corresponding to each ADO in 2001–2020 were calculated. This task allowed evaluating the variability of these parameters during ADO days of different intensity and on days without dust contribution.

Classification of synoptic atmospheric circulation patterns during ADO

Geopotential height fields at the 850 hPa level at 12 UTC from the NCEP/NCAR Reanalysis dataset were also downloaded and used to characterise the synoptic meteorological patterns that generated the atmospheric circulation at this level, during each day of the period 1948–2020. African dust is usually transported at heights at or above 1500 m above sea level over the IP-BI[25]. For this reason the evaluation of air-mass dynamics from 850 mb geopotential height maps has demonstrated to be a robust source of information to detect ADO[15–17,29,38].

Thereafter, a circulation classification methodology[39] was applied to group all days of the period 1948–2020 into a series of known characteristic patterns that occur frequently over SW Europe. The main patterns that give rise to African dust transport, which were obtained in the previous works[15,16,28,29] were also included. Thus, a non-hierarchical k-means cluster analysis was applied for classifying the geopotential height daily fields into similar groups, each one representing a circulation-type (CT) over this region[40]. A FORTRAN script was created to implement the

k-means cluster analysis. This software was able to choose the initial clusters, as well as obtaining the within-group and between-group variance in the output, according to the number of clusters selected[41,42]. The number of clusters to be retained was determined by computing the percentage change in the within-cluster variance, as a function of the number of the clusters. This statistic increases abruptly when clusters, which are significantly different are joined, helping to choose the best number of clusters to be retained[40].

Next, the association between the ADO identified over each region in 2001–2020 and the occurrence of specific CT was analyzed. The aim was to determine which of them triggered the development of these events more frequently (ADO CT). Besides, the variability of the levels of GT, TANOM and TPOT depending on the type of synoptic circulation was evaluated.

Trend analysis of ADO circulation patterns and thermodynamic parameters in the period 1948–2020

The results obtained so far have produced: 1) a list having all the days under ADO CT in the period 1948–2020; and 2) their associated daily mean values of TPOT, TANOM and GT in the 8 sub-domains. The above information was analyzed to check the occurrence of time trends using statistical methods. The "openair" data analysis package[43] adds a specific R function for calculating the trend in any numeric variable using the Theil-Sen method[44]. With this method it is possible to determine trends in time series of numerical values and to express the magnitude of the trend as a positive or negative slope indicating the increase or decrease of the analysed magnitude in units per year. The advantages of using this non-parametric approach are mainly that it tends to yield accurate confidence intervals even with non-normal data and heteroscedasticity. It is also resistant to the presence of outliers in the time series of data. Thus, trend

estimates of the number of days per year on which any of the ADO CT occurred over the whole period 1948–2020 were undertaken. Trend estimates were also performed for the mean values of TPOT, TANOM and GT over the IP-BI domain during days under ADO CT. Applied to monthly mean values, the method is insensitive to the existence of seasonality. Plots of smoothed trends for the monthly mean levels of thermodynamic parameters under ADO CT, were also determined with "openair" using the R function "smoothTrend". This function generates a plot of monthly levels and fit a smooth line to the data. The smooth line is essentially determined using Generalized Additive Modelling using the mgcv R package[45]. This package offers a flexible approach to calculating trends with the advantage that the amount of smoothness in the trend is optimised in the sense that it is neither too smooth (therefore missing important features) nor too variable (perhaps fitting 'noise' rather than real effects).

Statistical methods
Since not all groups of data fitted to normal distributions, several non-parametric tests (Mann-Whitney, Kolmogorov-Smirnoff and Kruskal-Wallis tests) were used to search for statistically significant differences between the medians and the shape of the distributions of 2 or more of them, for at least a 95% confidence level. 95% confidence intervals for the means and the medians were also determined using bootstrap resampling techniques. The Statgraphics Centurion XVII statistical software was used to perform these analyses. Bootstraping techniques were also used to quantify whether the trend estimates were statistically significant for a given confidence level with the "openair" data analysis tools[43].

DATA AVAILABILITY
In this study most data sets were obtained or calculated from open access repositories. This ensures the reproducibility of the procedures carried out in this study. Annual global fields of temperature and geopotential height at different pressure levels, used for the computation of the 3 thermodynamic parameters and for performing the circulation classification procedure, were downloaded from the National Centers for Environmental Prediction/National Centre for Atmospheric Research (NCEP/NCAR) Reanalysis dataset (http://www.esrl.noaa.gov/psd/data/) provided by NOAA/OAR/ESRL PSD, USA. Meteorological tools used to identify the occurrence of ADO over the Iberian Peninsula and the Balearic Islands can be obtained from these links: air mass back-trajectories (HYSPLIT trajectory model: https://www.arl.noaa.gov/hysplit/hysplit/), aerosol maps from numerical models (SKIRON - University of Athens: http://forecast.uoa.gr; DREAM/BSCDREAM8b - Barcelona Supercomputing Centre: https://ess.bsc.es/bsc-dust-daily-forecast; NAAPs - Naval Research Laboratory: https://www.nrlmry.navy.mil/aerosol/), satellite imagery (MODIS – NASA: http://modis.gsfc.nasa.gov/) and synoptic meteorological maps (NCEP/NCAR Reanalysis dataset: http://www.esrl.noaa.gov/psd/data/). Time series of PM_{10} levels registered at regional background monitoring sites in each area of study, used to estimate the daily dust contribution during ADO were provided by the Spanish Ministry of Ecological Transition. Restrictions apply to the availability of these data sets of air quality parameters registered at official air quality monitoring stations. Data are however available from the authors upon reasonable request and with permission of the Spanish Ministry of Ecological Transition. The procedure for identifying ADO and estimating the daily dust contribution to the regional background levels of PM_{10} can be obtained from: http://ec.europa.eu/environment/air/quality/legislation/pdf/sec_2011_0208.pdf and from: https://www.miteco.gob.es/images/es/metodologiaparaepisodiosnaturales-revabril2013_tcm30-186522.pdf. All these links were accessible on March 2022. In any case, all datasets generated during the current study are available from the corresponding author on reasonable request.

CODE AVAILABILITY
The FORTRAN software created for performing the circulation classification procedure is available from the corresponding author on reasonable request.

REFERENCES
1. Heffernan, O. The mystery of the expanding tropics. *Nature* **530**, 20–22 (2016).
2. Thomas, T. & Nigam, S. Twentieth-Century Climate Change over Africa: Seasonal Hydroclimate Trends and Sahara Desert Expansion. *J. Clim.* **31**, 3349–3370 (2018).
3. Zucca, C., Middelton, N., Kang, U. & Liniger, H. Shrinking water bodies as hotspots of sand and dust storms: The role of land degradation and sustainable soil and water management. *Catena* **207**, 105669 (2021).
4. Ginoux, P. et al. Global-scale attribution of anthropogenic and natural dust sources and their emission rates based on MODIS Deep Blue aerosol products. *Rev. Geophys* **50**, RG3005, https://doi.org/10.1029/2012RG000388 (2012).
5. Prospero, J. M. Saharan dust impacts and climate change. *Oceanography* **19**, 60–61 (2006).
6. Goudie A. S. & Middleton N. J. *Desert Dust in the Global System.* (Springer, Heidelberg, https://doi.org/10.1007/3-540-32355-4, 2006).
7. Prospero, J. M. & Lamb, P. J. African droughts and dust transport to the Caribbean: climate change implications. *Science* **302**, 1024–1027 (2003).
8. Sousa, P. M. et al. Saharan air intrusions as a relevant mechanism for Iberian heatwaves: The record breaking events of August 2018 and June 2019. *Weather. Clim. Extremes.* **26**, 100224 (2019).
9. Cruz, J. A., McDermott, F., Turrero, M. J., Edwards, R. L. & Martín-Chivelet, J. Strong links between Saharan dust fluxes, monsoon strength, and North Atlantic climate during the last 5000 years. *Sci. Adv.* **7**, eabe6102 (2021).
10. Alonso-Perez, S. et al. Trend changes of African airmass intrusions in the marine boundary layer over the subtropical Eastern North Atlantic region in Winter. *Tellus* **63B**, 255–265 (2011).
11. Varga, G. Changing nature of Saharan dust deposition in the Carpathian Basin (Central Europe): 40 years of identified North African dust events (1979–2018). *Environ. Int.* **139**, 105712 (2020).
12. Evan, A. T., Flamant, C., Gaetani, M. & Guichard, F. The past, present and future of African dust. *Nature* **531**, 493–495 (2016).
13. Querol, X. et al. Seasonal evolution of suspended particles around a large coal-fired power station: particulate levels and sources. *Atmos. Environ.* **32**, 1963–1978 (1998).
14. Querol, X. et al. African dust contributions to mean ambient PM10 mass-levels across the Mediterranean Basin. *Atmos. Environ.* **43**, 4266–4277 (2009).
15. Pey, J., Querol, X., Alastuey, A., Forastiere, F. & Stafoggia, M. African dust outbreaks over the Mediterranean Basin during 2001-2011: PM_{10} concentrations, phenomenology and trends, and its relation with synoptic and mesoscale meteorology. *Atmos. Chem. Phys.* **13**, 1395–1410 (2013).
16. Escudero, M. et al. Wet and dry African dust episodes over Eastern Spain. *J. Geophys. Res.* **110**, D18S08 10.1029 (2005).
17. Salvador, P. et al. African dust contribution to ambient aerosol levels across central Spain: Characterization of long-range transport episodes of desert dust. *Atmos. Res.* **127**, 117–129 (2013).
18. Pérez, L. et al. Coarse particles from Saharan dust and daily mortality. *Epidemiology* **19**, 800–807 (2008).
19. Pérez, L. et al. Effects of local and Saharan particles on cardiovascular disease mortality. *Epidemiology* **23**, 768–769 (2012).
20. Stafoggia, M. et al. Desert dust outbreaks in southern Europe: contribution to daily PM10 concentrations and short-term associations with mortality and hospital admissions. *Environ. Health Perspect.* **124**, 413–419 (2016).
21. Díaz, J. et al. Saharan dust intrusions in Spain: health impacts and associated synoptic conditions. *Environ. Res.* **156**, 455–467 (2017).
22. Ridame, C. et al. Contrasted Saharan dust events in LNLC environments: impact on nutrient dynamics and primary production. *Biogeosciences* **11**, 4783–4800, https://doi.org/10.5194/bg-11-4783-2014 (2014).
23. Pérez-Martínez, C., Rühland, K. M., Smol, J. P., Jones, V. J. & Conde-Porcuna, J. M. Long-term ecological changes in Mediterranean mountain lakes linked to recent climate change and Saharan dust deposition revealed by diatom analyses. *Sci. Total Environ.* **727**, 138519 (2020).
24. Querol, X. et al. *Procedimiento Para Identificación de Episodios Naturales Africanos de PM₁₀ y PM₂.₅, y la Demostración de Causa en lo Referente a las Superaciones del Valor Límite Diario de PM₁₀.* (Scientific Report published by the Spanish Ministry of Agriculture, Food and Environment and the Portuguese Environmental Agency, Madrid, Spain) Available online at: https://www.miteco.gob.es/images/es/metodologiaparaepisodiosnaturales-revabril2013_tcm30-186522.pdf (Last access March 2022). (2013).
25. Querol, X. et al. Monitoring the impact of desert dust outbreaks for air quality for health studies. *Environ. Int.* **130**, 104867 (2019).
26. Escudero, M. et al. A methodology for the quantification of the net African dust load in air quality monitoring networks. *Atmos. Environ.* **41**, 5516–5524 (2007).
27. Commission staff working paper, establishing guidelines for demonstration and subtraction of exceedances attributable to natural sources under the Directive 2008/50/EC on ambient air quality and cleaner air for Europe, Brussels, 15.02.2011. SEC(2011) 208 final.
28. Rodríguez, S., Querol, X., Alastuey, A., Kallos, G. & Kakaliagou, O. Saharan dust contributions to PM10 and TSP levels in Southern and Eastern Spain. *Atmos. Environ.* **35**, 2433–2447 (2001).

29. Salvador, P. et al. African dust outbreaks over the western Mediterranean basin: 11 year characterization of atmospheric circulation patterns and dust source areas. *Atmos. Chem. Phys.* **14**, 6759–6775 (2014).

30. Marshall, J. North Atlantic climate variability: phenomena, impacts and mechanisms. *Int. J. Climatol.* **21**, 1863–1898 (2001).

31. Gillet, N. P., Graf, H. F. & Osborn, T. J. Climate Change and the North Atlantic Oscillation. *Chapter in The North Atlantic Oscillation: Climatic Significance and Environmental Impact* (Published by the American Geophysical Union as part of the Geophysical Monograph Series, **134**., Washington, DC, Editor(s): Hurrell, J. W., Kushnir, Y., Ottersen, G. & Visbeck, M.), https://doi.org/10.1029/134GM09 (2003).

32. Masson-Delmotte, V. et al. *IPCC, 2021: Climate Change 2021: The Physical Science Basis. Contribution of Working Group I to the Sixth Assessment Report of the Intergovernmental Panel on Climate Change* (Cambridge Univ. Press. In press).

33. Viana, M. et al. Assessing the performance of methods to detect and quantify African dust in airborne particulates. *Environ. Sci. Technol.* **44**, 8814–8820 (2010).

34. Kalnay, E. et al. The NCEP/NCAR 40-year reanalysis project. *B. Am. Meteorol. Soc.* **77**, 437–470 (1996).

35. Wallace, J. M. & Hobbs, P. V. *Atmospheric Science – an Introductory Survey*, second ed. (Elsevier, Canada, 2006).

36. Galvin, J. F. P. *An Introduction to the Meteorology and Climate of the Tropics.* (Wiley-Blackwell, West Sussex, UK, 2016).

37. Sánchez-Benítez, A., García-Herrera, R., Barriopedro, D., Sousa, P. M. & Trigo, R. M. June 2017: The Earliest European Summer Mega-heatwave of Reanalysis Period. *Geophys. Res. Lett.* **45**, 1955–1962 (2018).

38. Salvador, P., Artíñano, B., Querol, X. & Alastuey, A. A combined analysis of backward trajectories and aerosol chemistry to characterise long-range transport episodes of particulate matter: The Madrid air basin, a case study. *Sci. Total Environ.* **390**, 495–506 (2008).

39. Huth, R. et al. Classifications of atmospheric circulation patterns. *Ann. Ny. Acad. Sci.* **1146**, 105–152 (2008).

40. Belis, C. et al. *European Guide on Air Pollution Source Apportionment with Receptor Models*, EUR 29816 EN, Publications Office of the European Union, Luxembourg, ISBN 978-92-76-09001-4, https://doi.org/10.2760/439106, JRC117306 (2019).

41. Salvador, P., Barreiro, M., Gómez-Moreno, F. J., Alonso-Blanco, E. & Artíñano, B. Synoptic classification of meteorological patterns and their impact on air pollution episodes and new particle formation processes in a south European air basin. *Atmos. Environ.* **245**, 118016 (2021).

42. von Schneidemesser, E. et al. Learning from the COVID-19 lockdown in berlin: Observations and modelling to support understanding policies to reduce NO_2. *Atmos. Environ.: X* **12**, 100122 (2021).

43. Carslaw, D. C. & Ropkins, K. Openair - an R package for air quality data analysis. *Environ. Modell. Softw.* **27-28**, 52–61 (2012).

44. Hirsch, R., Slack, J. R. & Smith, R. A. Techniques of trend analysis for monthly water quality data. *Water Resour. Res* **18**, 107–121 (1982).

45. Carslaw, D. C., Beevers, S. D. & Tate, J. E. Modelling and assessing trends in traffic related emissions using a generalised additive modelling approach. *Atmos. Environ.* **41**, 5289–5299 (2007).

ACKNOWLEDGEMENTS

AUTHOR CONTRIBUTIONS

P.S.: Conceptualization; Methodology; Software; Formal analysis; Investigation; Data Curation; Writing - Original Draft; Visualization; J.P.: Conceptualization; Methodology; Formal analysis; Investigation; Resources; Writing - Review & Editing; Project administration; Funding acquisition; N.P.: Methodology; Formal analysis; Investigation; Data Curation; Writing - Review & Editing; X.Q.: Methodology; Formal analysis; Investigation; Resources; Writing - Review & Editing; Supervision; B.A.: Methodology; Formal analysis; Investigation; Resources; Writing - Review & Editing; Supervision.

COMPETING INTERESTS

The authors declare no competing interests.

ADDITIONAL INFORMATION

Supplementary information The online version contains supplementary material available at https://doi.org/10.1038/s41612-022-00256-4.

Correspondence and requests for materials should be addressed to Pedro Salvador.

Reprints and permission information is available at http://www.nature.com/reprints

Publisher's note Springer Nature remains neutral with regard to jurisdictional claims in published maps and institutional affiliations.